

New thermal optimization scheme of power module in solid-state amplifier

Lie-Peng Sun¹ · Zhen-Yu Yuan¹ · Cheng Zhang¹ · Xian-Bo Xu³ · Jun-Gang Miao² · Jian-Hua Zhang¹ · Long-Bo Shi³ · Yuan He³

Received: 22 May 2018/Revised: 17 September 2018/Accepted: 19 October 2018/Published online: 25 March 2019
© China Science Publishing & Media Ltd. (Science Press), Shanghai Institute of Applied Physics, the Chinese Academy of Sciences, Chinese Nuclear Society and Springer Nature Singapore Pte Ltd. 2019

Abstract The new 1 kW power module for ADS project needs the optimization of cooling design including water flow and tunnel layout, and the water flow of three tons per hour was chosen to be a goal for a 20 kW power source. According to analysis from the insertion and integrated loss, about 24 modules were integrated into the rated power. Thus, every module has a cooling flow of 2.1 L/min for RF heat load and power supply loss, which is very hard to achieve if no special consideration and techniques. A new thermal simulation method was introduced for thermal analysis of cooling plate through CST multi-physics suite, especially for temperature of power LDMOS transistor. Some specific measures carried out for the higher heat transfer were also presented in this paper.

Keywords RF system · Solid-state amplifier · Power module · Heat transfer coefficient

1 Introduction

The China-ADS project (“Strategic Priority Research Program” of the Chinese Academy of Sciences) was launched in 2011 to pursue the R&D on key technologies toward a final demonstration facility on ADS with the capability of more than 1000 MW thermal power. The driver proton linear accelerator is defined to have 25 MeV energy, 10 mA current, and in CW operation mode. It employs superconducting structures except the radio frequency quadrupole (RFQ) [1].

In 2014, the continuing 10 mA proton was accelerated to reach up to 2.1 MeV inside RFQ successfully in IMP, and after that RF system has been updated few times for stable and secure operation. The original power source was a tetrode amplifier without circulator, which is a potential risk while the high-intensity current beam passed the RF structure resulting in influencing its eigenfrequency. The newest RF system was constituted of two 80 kW solid-state amplifiers with many small circulators inserted in power modules for feeding power to a separate coupler (shown in Fig. 1), and the frequency was stabilized through adjusting the temperature of the inlet water, whose operating scheme needs to be analyzed carefully by beam loading.

A new 80 kW solid-state amplifier from BBEF was installed and measured for the performance test, and the power from four identical 22 kW cabinets was combined to the rating power of 80 kW. The amplifying link is presented in Fig. 2.

For ADS project requirements, the cooling flow of hundreds of amplifiers would be excessive to be supplied if no optimization was conducted. Thus, all thermal optimization should be considered to improve the heat transfer on the power module. In fact, the Microwave Studio

This work was supported by the “strategic priority research program” of the Chinese Academy of Sciences (No. XDA030205).

✉ Lie-Peng Sun
sunnyslp@163.com

¹ Beijing BBEF Science and Technology Co., Ltd.,
Beijing 101312, China

² Beihang University, Beijing 100082, China

³ Institute of Modern Physics, Chinese Academy of Sciences,
Lanzhou 730000, China

simulation aimed at a power module to focus on several thermal boundaries' configuration other than some specific heat transfer code such as Flotherm and HSC Chemistry. One important reason calculated by Microwave Studio was all simulation in it, which can switch conveniently between the electro-magnetic and multi-physics solvers based on the finite integral method. A special test bench was installed for RF characteristic and thermal measurements shown in Fig. 3.

The layout of the cooling channel was considered according to the thermal requirements and fabrication cost. BLF188XR remains one of the most popular power transistors considering the rating power and frequency; the distribution of the cooling channel is shown in Fig. 4 according to the thermal loss related to the operating status [2] and its location.

2 Thermal simulation background [3]

For thermal simulation, its theory and method were also deduced and verified in some books and journals; the journal [4] provides it in detail. A cooling water velocity v is 2.25 m/s (7.38 ft/s) in the inlet pipe according to the measurement, an estimation of the pressure drop gives a value of approximately 0.8 bar, and the specific heat capacity [5] of water C_p equals to 4200 J/(kg K) and the temperature of inlet water is nearly 20 °C, the water density d is:

$$d = -0.2162T + 1002. \tag{1}$$

In addition, the viscosity u (Pa s) in channel [6] was obtained through:

$$u = -2.5225 \times 10^{-5}T + 1.5125 \times 10^{-3} \tag{2}$$

Calculating the heat transfer coefficient h (W/(m² K)) [7] for an annular channel is complex, but an approximation can be obtained by substituting in the expressions for the Reynolds Re and Prandtl numbers Pr (both dimensionless) [8].

$$Pr = -0.198T + 10.964 \tag{3}$$

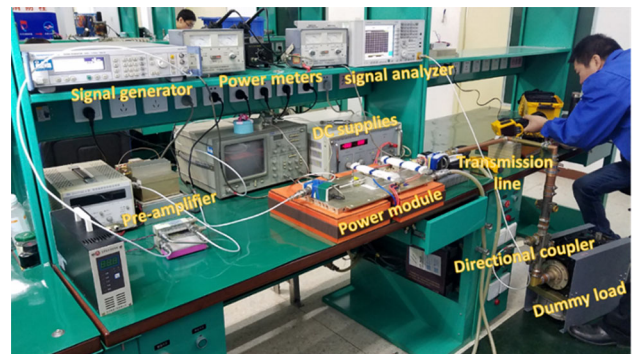


Fig. 3 (Color online) RF measurement workbench with all types of module sub-systems

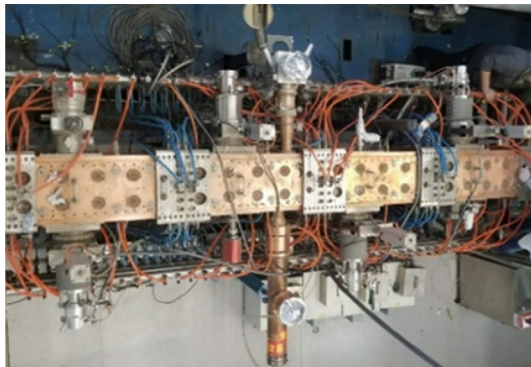


Fig. 1 (Color online) RFQ cavity and its coupler's layout

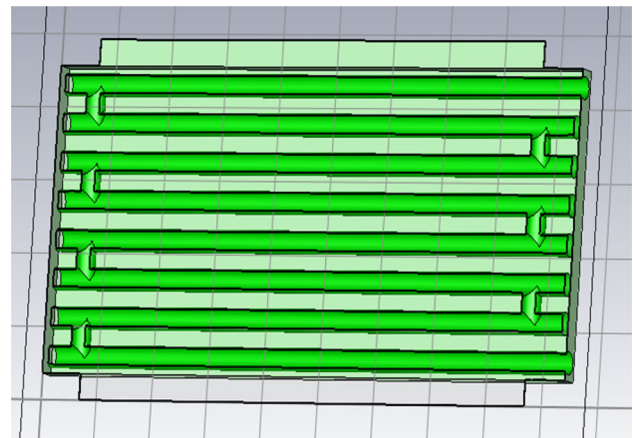


Fig. 4 (Color online) Simple layout of cooling channels resulting from RF characteristic of power transistor

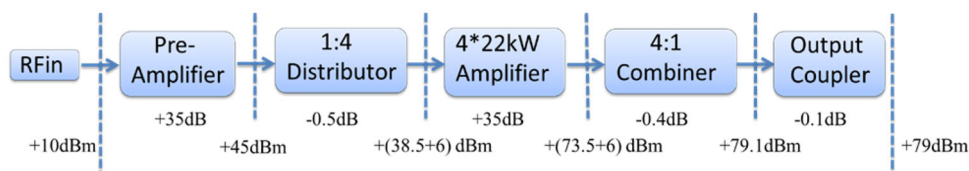


Fig. 2 Amplifying link of BBEF 80 kW solid-state amplifier (SSA)

The coaxial cooling channel has an equivalent radius $r = 0.004$ m, for a viscosity $\mu = 0.9 \times 10^{-3}$ kg/ms, density $\rho = 1000$ kg/m³, and a velocity of 4.6 m/s in the annulus; the Reynolds number is [9]:

$$Re = d \cdot v \cdot 0.3048 \cdot 2r/\mu \quad (4)$$

For forced convection in a closed conduit, the Nusselt number, Nu , is given by modified Dittus–Boelter equation for turbulent flow [10]:

$$Nu = 0.023Re^{0.8}Pr^{0.4} \quad (5)$$

With the thermal conductivity [11] of water k (W/(m K)):

$$k = 0.00162T + 0.56977 \quad (6)$$

The heat transfer coefficient [12] is given by:

$$h = 0.5kNu/r, \quad (7)$$

thus remembering that the initial values on site allow h to be estimated easily from formulas as above which is 9490 W/(m K). Moreover, in the simulation, the 18 °C ambient temperature for power transistor heat transfer from air was also considered simultaneously [13]. Further, while the output power reaches up to 110 W without cooling, a complete temperature cloud map of the power module was obtained using Fluke infrared thermometer 572, shown in Fig. 5.

3 Thermal simulation

For thermal simulation in this example, the thermal parameters of different materials shown in Table 1 were examined carefully for solver running, and especially for CST, the thermal boundaries were considered and set according to the simulation requirements; the different

configurations may affect the final calculated value other than ANSYS code. In addition, it should be noted that the heat exchange comes from not only the cooling water but also air on the entire exposed surface of module structure.

The simulation results under this circumstance with CST thermal solver are presented in Fig. 6. Some special parameter configuration was considered carefully because of software particularities. First, the thermal boundaries [14] were set to open add space and 0.1 distance factor from ambient according to the journal. Second, except the major heat exchange via water channels [15] in cooling plate, the heat transfer from surroundings cannot be easily ignored, which according to the experiences and examples was approximately 20 on each and every face exposed in air. Finally, the only heat source was the power transistor, whose heat volume or density may be obtained from the output efficiency of LDMOS; when the maximum output power reaches up to 110 W, the dissipation power on the transistor would increase to approximately 400 W due to the low RF transfer efficiency.

A maximum temperature of 56.8 °C was observed on the power transistor without water cooling. Moreover, when we turn on the water valve, the temperature clearly decreases instantly, and the experiment and simulated results are shown in Fig. 7a, b, respectively, which indicates good agreement between the simulated value and the measurement.

4 Comparison between different thermal simulation codes

When 200 W output power was observed in the power meter, the temperature of conducting plate is approximately 102 °C without cooling water. Since it is rigidly bolted to the

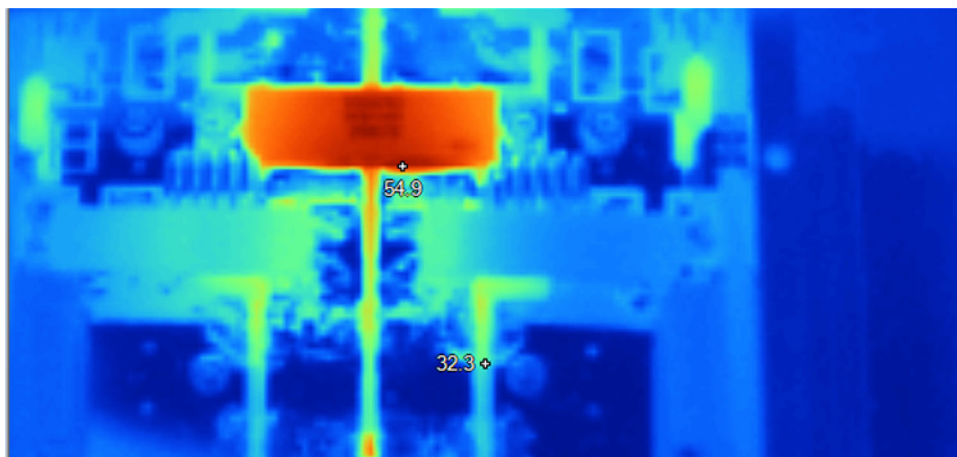
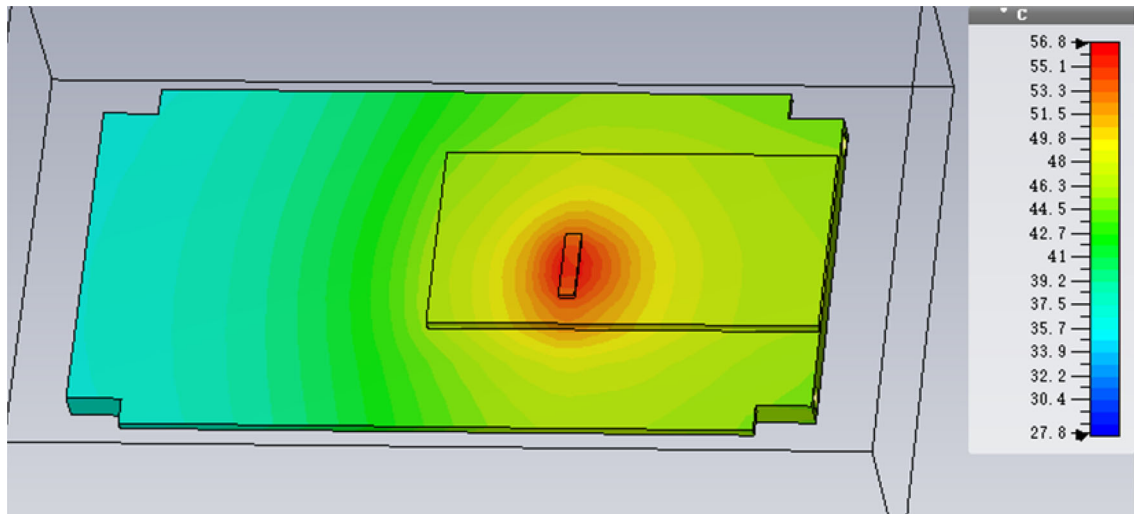
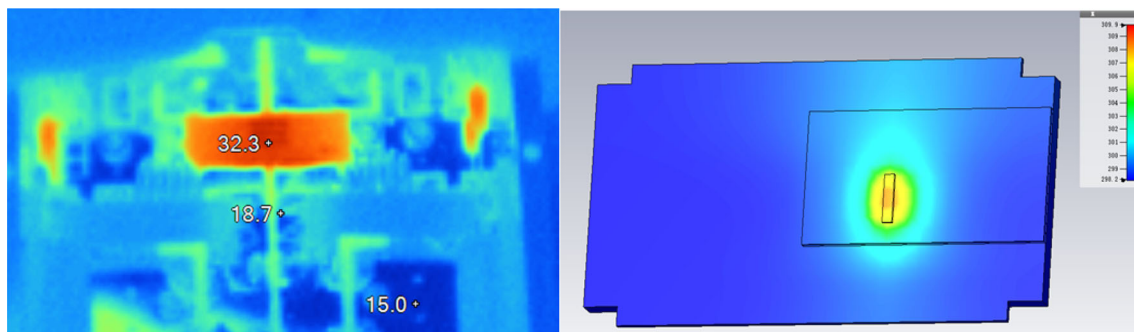


Fig. 5 (Color online) Temperature distribution map from thermometer with 110 W output power

Table 1 Parameters lists of the related materials

Material	Thermal conductivity (W/K m)	Heat capacity (kJ/K kg)	Density (kg/m ³)
Aluminum	237.0	0.9	2700
Copper	401	0.39	8930
Water	0.6	4.2	1000
Air	0.026	1.005	1.204

**Fig. 6** (Color online) Simulation results in the same conditions as that of the measurements**Fig. 7** (Color online) **a** Temperature cloud map in Fluke thermometer while the water turns on (left). **b** Simulated value with cooling channel under the same circumstance (right)

cooling plate, where there is no condition for thermal exchange except for air. This temperature gradient produces a maximum movement on the longer leg and is in the order of + 0.2 mm in the 'Y' axis, i.e., vertically upward. A full-scale power module is used as a test piece to verify the finite element model. Moreover, this real power module applies a measured heat load with 2.3 L/min running through the cooling channel. One thermocouple was used to monitor the surface temperature below the MOSFET.

The finite element software ANSYS [16] is used to check the exact conditions of the test and CST-simulated results.

Applying the same heat load to the finite element model and using the revised heat transfer coefficients [17] with a staggered bulk fluid, the RF heat has an extra temperature increase, and the two softwares have a good agreement in Fig. 8, which shows temperatures of 56–116 °C from ANSYS within 12% of the simulated values from CST.

When water valve was turned on, the maximum temperature of heat plate drops to a more acceptable operational level. This temperature drop, by definition, decreases the distortion of the whole structure.

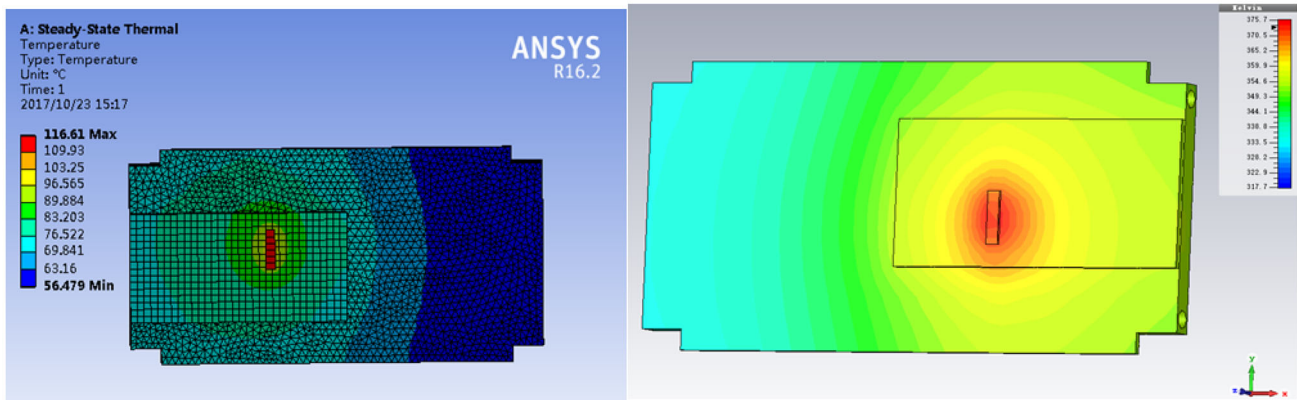


Fig. 8 (Color online) Temperature cloud map of maximum power using ANSYS (left) and CST (right)

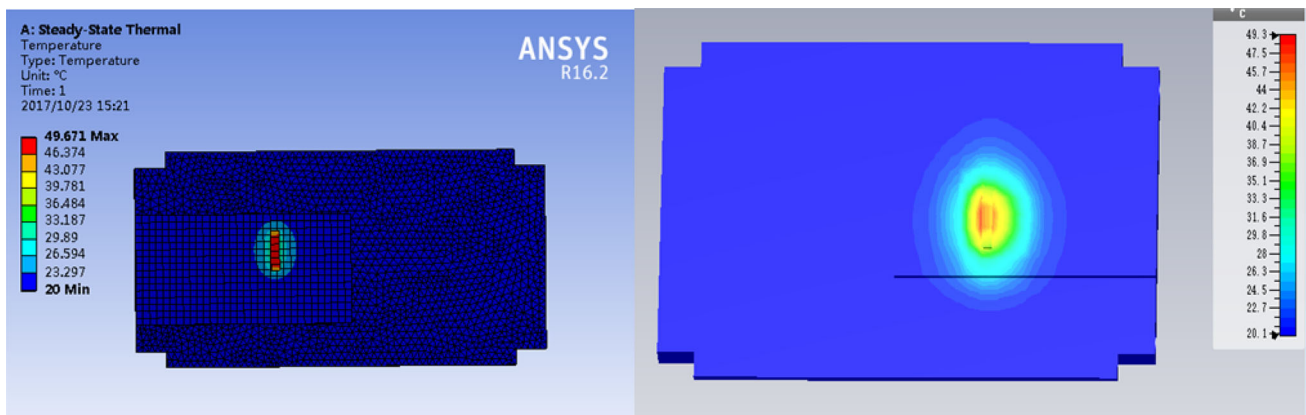


Fig. 9 (Color online) Temperature cloud map of maximum power using ANSYS (left) and CST (right)

As a famous simulation code in the region of accelerator, ANSYS results were considered to be precise and reasonable. Figure 9 shows a good agreement between the two codes. A final note about CST simulation is that it indicates the configuration of complicated thermal boundaries, and the heat exchange was verified according to the situation on site.

5 Cooling performance optimization

The experimental results show satisfactory agreement between the different codes and provide confidence in its use for further developments. Moreover, some new structures would apply to the higher cooling requirements, which focused on higher efficiency of heat transfer and exchange [18] on the location of special components, such as the power transistor and observed load. Figure 10 shows

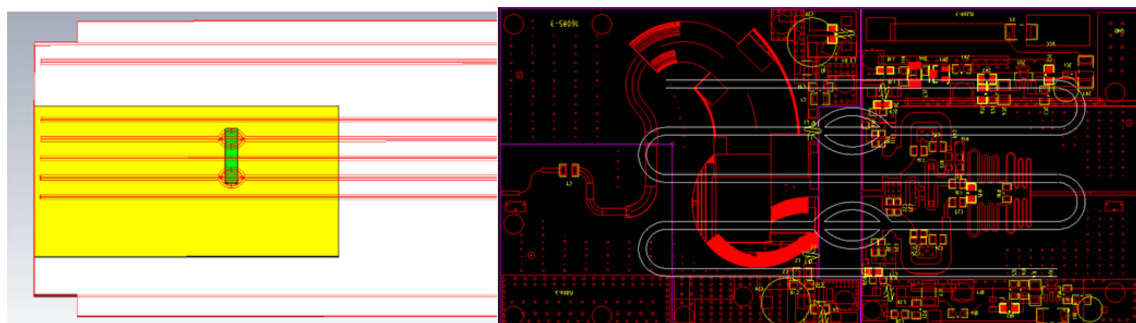


Fig. 10 (Color online) Overview of multi-layer cooling structure in the simulated software (left). The construction drawing of cooling design for the power transistor (right)

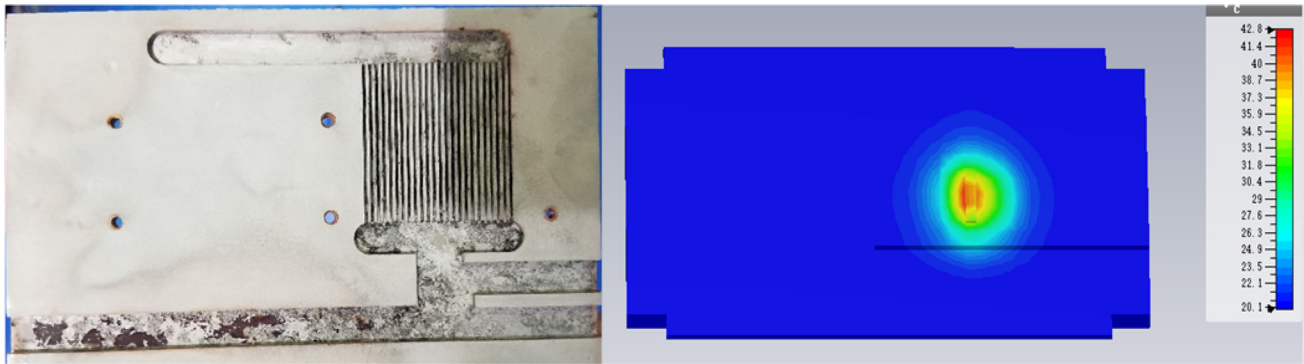


Fig. 11 (Color online) Cross section of fin-fan structure (left) and its cooling performance (right)

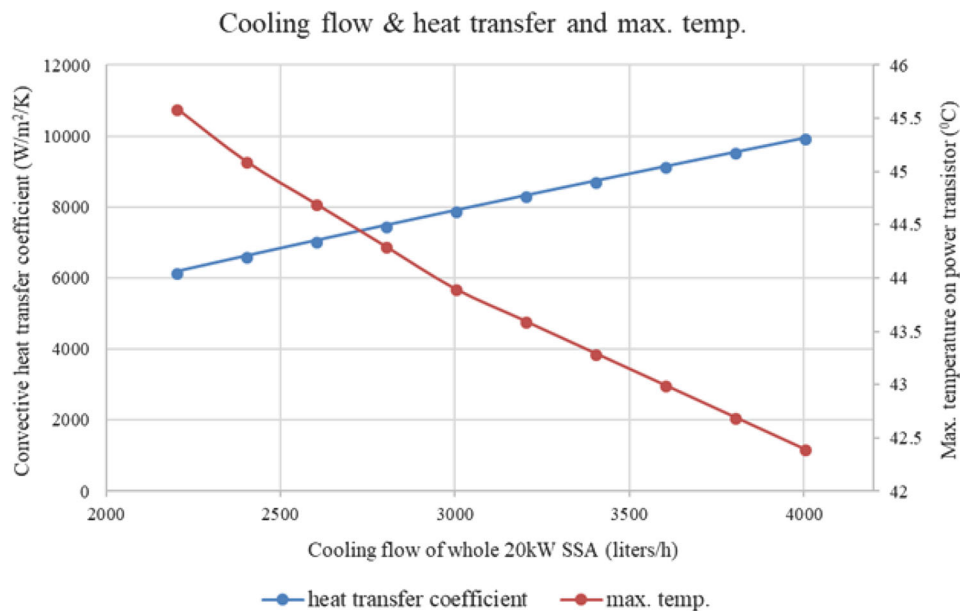


Fig. 12 Relationship between the flow requirement of whole amplifier and thermal simulation

the multi-layer cooling channels concentrated on power transistor, and the temperature cloud map indicates that the better effect can be verified compared with the ordinary design of the cooling channels.

The fin-fan structure was more complicated and effective for cooling performance, which is shown in Fig. 11. However, its fabrication is difficult and the cost would be high due to welding process and surface treatment process. Under the same heat load circumstance, the maximum temperature was lower than the non-fin structure.

6 Conclusion

According to the analysis and simulation results above, the optimization of cooling performance was conducted for higher heat transfer efficiency and lower operating temperature, which is shown in Fig. 12. The goal of the accelerator facility in the future is a more robust design of the amplifier system, which can consider the balance of operating stability from amplifier and more economical cooling water supply, and new optimization design in microstructure was tested through the welding and anti-corrosion process.

Moreover, from the fundamental design of the whole machine cooling on heat load in each and every power module, some professional-grade software tools can easily be applied for thermal simulation, such as CST (based on

the finite integral method) and ANSYS (based on the finite element method). Due to the first-time simulation on cooling plate performance using them, the different simulated results were the excellent cross-check for correctness. In addition, these professional codes can mutually switch between the microwave and multi-physics solvers for more precise and convenient simulation.

Finally, the cooling performance was improved through some special microchannels, such as the fin-fan structure. Considering the design of water flow, the significant fluctuation of the transfer coefficient indicates the cooling optimization in structure achieving a desired or significant effect on the whole design range of water flow.

References

- J.Y. Tang, P. Cheng, H.P. Geng, et al., Conceptual physics design for the China-ADS LINAC, in *Paper Presented at the 2nd North American Particle Accelerator Conference (THPSM04)*, Pasadena Convention Center, Pasadena, 29. Sept 4, 2013
- BLF188XR; BLF188XRS (Product data sheet, 2013), <http://ampleon.com>. Accessed 12 Sept 2013
- T.L. Bergman, A.S. Lavine, F.P. Incropera et al., *Fundamentals of Heat and Mass Transfer*, 7th edn. (Wiley, Hoboken, 2011), pp. 675–679
- G.R. Murdoch, H. Vormann, Thermal design of an RFQ cell for the radio frequency quadrupole under construction for ISIS, in *Paper Presented at the 6th European Particle Accelerator Conference (TUP42G)*, City Conference Centre, Stockholm, 22–26 June 1998
- M.H. Anderson, L.E. Herranz, M.L. Corradini, Experimental analysis of heat transfer within the AP600 containment under postulated accident conditions. *Nucl. Eng. Des.* **185**(2), 153–172 (1998). [https://doi.org/10.1016/S0029-5493\(98\)00232-5](https://doi.org/10.1016/S0029-5493(98)00232-5)
- G. Neils, S. Kliein, *Heat Transfer* (Cambridge University Press, Cambridge, 2009), pp. 799–806
- X.Y. Wei, X.D. Fang, R.R. Shi, A comparative study of heat transfer coefficients for film condensation. *Energy Sci. Technol.* **3**(1), 1–9 (2012). <https://doi.org/10.3968/j.est.1923847920120301.152>
- G.M. Hebbard, W.L. Badger, Steam-film heat transfer coefficients for vertical tubes. *Ind. Eng. Chem.* **26**(4), 420–424 (1934). <https://doi.org/10.1021/ie50292a013>
- M.H. Kim, M.L. Corradini, Modeling of condensation heat transfer in a reactor containment. *Nucl. Eng. Des.* **118**(2), 193–212 (1990). [https://doi.org/10.1016/0029-5493\(90\)90057-5](https://doi.org/10.1016/0029-5493(90)90057-5)
- B. Zhang, J.Q. Shan, J. Jiang et al., Simulation of heat transfer of supercritical water in obstacle-bearing vertical tube. *Nucl. Sci. Technol.* **21**, 241–245 (2010). <https://doi.org/10.13538/j.1001-8042/nst.21.241-245>
- L.E. Herranz, A. Campo, Adequacy of the heat-mass transfer analogy to simulate containment atmospheric cooling in the new generation of advanced nuclear reactors: experimental confirmation. *Nucl. Technol.* **139**(3), 221–232 (2002). <https://doi.org/10.13182/NT02-A3315>
- W.J. Minkowycz, E.M. Sparrow, Condensation heat transfer in the presence of noncondensables, interfacial resistance, superheating, variable properties, and diffusion. *Int. J. Heat Mass Transf.* **9**(10), 1125–1144 (1966). [https://doi.org/10.1016/0017-9310\(66\)90035-4](https://doi.org/10.1016/0017-9310(66)90035-4)
- W.M. Rohsenow, Heat transfer and temperature distribution in laminar film condensation. *Trans. ASME* **78**, 1645–1648 (1956)
- H. Wang, F. Shi, H. Zhu et al., Thermal boundary conditions in multiphysics algorithm for semiconductor device simulation. *High Power Laser Part. Beams* (2016). <https://doi.org/10.11884/hplpb201628.160129>. (in Chinese)
- W.S. Janna (ed.), *Engineering Heat Transfer*, 3rd edn. (Springer, New York, 2010)
- ANSYS/EM Elements User's Manual. <https://www.yumpu.com/.../view/16905502/element-tables-ansys-users>. Accessed 14 Sept 2000
- J.F. Jin, H.B. Chen, W.L. Xiao et al., Heat transfer analysis of bent cooling channels in SRF light-blocked components. *Nucl. Sci. Technol.* **23**, 321–327 (2012). <https://doi.org/10.13538/j.1001-8042/nst.23.321-327>
- Y. Li, C.Q. Yan, Z.N. Sun et al., Pool boiling heat transfer enhancement on porous surface tube. *Nucl. Sci. Technol.* **22**, 122–128 (2011). <https://doi.org/10.13538/j.1001-8042/nst.22.122-128>